2nd International Conference on Engineering Optimization
September 6 - 9, 2010, Lisbon, Portugal

Determining thermal contact resistance of the fin-to-tube attachment in plate fin-and-tube heat exchanger

Dawid Taler[1], Artur Cebula[2]

[1] Academy of Science and Technology, Cracow, Poland, taler@imir.agh.edu.pl
[2] Cracow University of Technology, Cracow, Poland, acebula@pk.edu.pl

Abstract
Plate fin-and-tube heat exchangers are made by inserting oval tubes through sheet metal strips with stamped holes and then expanding the tubes slightly to cause pressure at the tube-to-strip contacts. The gap between the fin base and the outer tube surface may be filled with air or corrosion products causing a decline in the ability of plate fins to transfer heat. The contact resistance must be accounted for in the design and performance calculations of heat exchangers. In this paper, the thermal contact resistance of the fin-to-tube attachment is estimated from the condition that the dimensionless correlations for the Colburn j-factors obtained from two different methods are in good agreement. The first method is based on the experimental data, while the second one on the CFD simulation of the flow and heat transfer in the heat exchanger.
Keywords: heat exchangers, fin-and-tube heat exchanger, CFD, heat transfer

1. Introduction

Externally finned tubes, or plate-and-tube elements are used in economizers of steam power boilers, air-conditioning heat exchangers, convectors for home heating, induced-draft cooling towers, and waste-heat recovery systems for gas turbines. Plate-and-tube extended surfaces are also used extensively in air-fin coolers, in which a hot fluid flows within the tubes, and atmospheric air, serving as the cooling fluid, is circulated over the fins by fans. The plate fin-and-tube heat exchangers are made by inserting the oval tubes through sheet metal strips with stamped holes and then expanding the tubes slightly to cause pressure at the tube-to-strip contacts. If the tubes are only expanded into the plates to produce "an interference fit" some contact resistance must be accounted for. In the design of plate fin-and-tube heat exchangers, contact resistance has been included in air-side resistance as a consequence of the data reduction methods used. The thermal contact resistance between fins and tubes has not been studied deeply owing to the complexity of heat transfer through rough metallic interfaces. The contact resistance in a fin-and-tube heat exchanger has been studied by Dart [1]. In his method, hot water flows through one tube row and cold water through an adjacent tube row. The estimated thermal contact resistance was compared to that in soldered fins. The Dart method was refined by Sheffield et. al.[2]. Convective heat dissipation on the fin surface and convective heat transfer between hot and cold tubes were eliminated by testing plate finned heat exchangers in a vacuum chamber. The heat is transferred radially from the hot water tubes to the cold water tubes only by conduction through the fins. Two-dimensional temperature distribution in the fin was determined using an electrically conducting paper model of the fin. Similar techniques were used by Jeong at al.[3,4]. Also, the investigated fin-and-tube heat exchanger was placed in an insulated vacuum chamber, thereby improving the accuracy of the numerical procedure for determination of the thermal contact resistance. On the other hand, heat transfer conditions on the fin surface and in the gap between fin and tube in vacuum differ from those in actual heat exchangers. In this study, a new experimental-numerical technique is developed for the estimation of the thermal contact resistance of plate finned tubes. The air side heat transfer coefficient is determined from the condition that the air temperature differences across the heat exchanger obtained from the CFD simulation and from the analytical model of the heat exchanger are equal. Based on the calculated heat transfer coefficients, the dimensionless correlations for the Colburn j-factor as a function of the Reynolds number and the thermal contact resistance are found. The thermal contact resistance of the fin-to-tube attachment is estimated from the condition that the dimensionless correlations for the Colburn j-factors obtained from the first and second method are in good agreement.

2. Thermal design of fin-and-tube heat exchanger

The basic equation for the total rate of heat transfer $\dot{Q}$ in a cross-flow tube heat exchanger is

$$\dot{Q} = F\, A_o U_o \Delta T_{lm} \tag{1}$$

where F is the correction factor based on logarithmic mean temperature difference ΔT_{lm} for a counterflow arrangement and A_o is the total external surface area of the tubes without fins (Fig. 1) on which the overall heat

transfer coefficient U_o is based.
The overall heat transfer coefficient referred to the surface area A_o is given by

$$\frac{1}{U_o} = \frac{A_o}{A_{in}} \frac{1}{h_{in}} + \frac{2A_o}{A_{in} + A_o} \frac{\delta_t}{k_t} + \frac{1}{\overline{h}_a} \frac{A_o}{A_g} + R_c \tag{2}$$

where R_c is the contact thermal resistance between the fins and tube, which is calculated from

$$R_c = \frac{2A_o}{A_o + A_g} \frac{g}{k_g} \tag{3}$$

The symbols δ_t and k_t denote the thickness and thermal conductivity of the tube, respectively and h_{in} the heat transfer coefficient on the tube inner surface. The equivalent, enhanced air-side heat transfer coefficient $\overline{h}_a$ based on the outer surface area A_o of the plain tube is defined as:

$$\overline{h}_a = \frac{A_f \eta_f (h_a) + A_w}{A_g} h_a \tag{4}$$

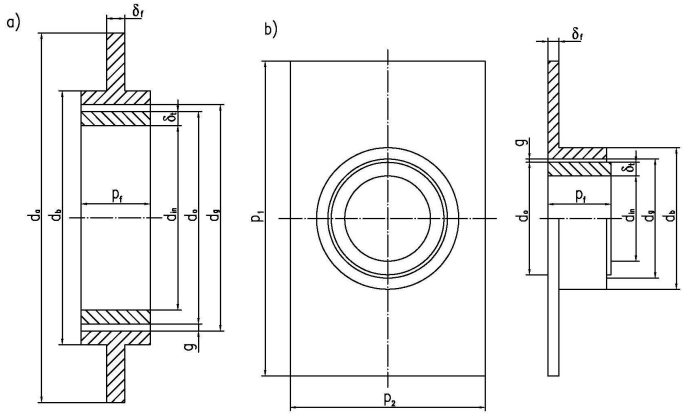

Figure 1: Nomenclature for the analysis of thermal contact resistance between the tube and fin; (a) integral fin extruded from tube (muff-type attachment), (b) L-footed attachment

where A_f is the external area of the fins, A_w is the external surface of the tube between fins and η_f is the fin efficiency [5-8]. Equation (4) is valid for various fin-to-tube attachments: tension-wound, L-footed, and integral fin extruded from tube. The air-side heat transfer coefficient h_a is calculated from experimental correlations for finned or plate-finned tube arrangements. This coefficient can be also calculated from correlations based on the CFD simulation of the flow and heat transfer in the heat exchanger. The procedure for determining a contact thermal resistance R_c (Eq. (3)) is presented in the following.

3. Characteristics of the tested heat exchanger

The tested automotive radiator is used for cooling the spark ignition engine with cubic capacity of 1,580 cm^3. The cooling liquid warmed up by the engine is subsequently cooled down by air in the radiator. The radiator consists of 38 tubes of an oval cross-section, 20 of them located in the upper pass and 10 tubes per row (Fig. 2). In the lower pass, there are 18 tubes with 9 tubes per row. The radiator is 520 mm wide, 359 mm high and 34 mm thick. The outer diameters of the oval tubes are d_{min} = 6.35 mm and d_{max} = 11.82 mm. The thickness of the tube wall is δ_t = 0.4 mm. The total number of plate fins equals 520. The dimensions of the single tube plate are as follows: length - 359 mm, height - 34 mm and thickness - δ_f = 0.08 mm. The plate fins and the tubes are made of aluminum. The path of the coolant flow is U-shaped. The two rows of tubes in the first (upper) pass are fed simultaneously from one header. The water streams from the first and second row are mixed in the intermediate header. Following that, the water is uniformly distributed between the tubes of the first and second row in the second (lower) pass (Fig. 3). The inlet, intermediate and outlet headers are made of plastic. The pitches of the tube arrangement are as follows: perpendicular to the air flow direction p_1=18.5 mm and longitudinal p_2=17 mm. A smooth plate fin is divided into equivalent rectangular fins. The efficiency of the fin was calculated by means of the Finite Volume Method. The hydraulic diameter of an oval tube is calculated using the formula $d_t = 4\,A_{in}\,/P_{in}$ where A_{in} is the area of the tube cross section and P_{in} is the inside tube perimeter.

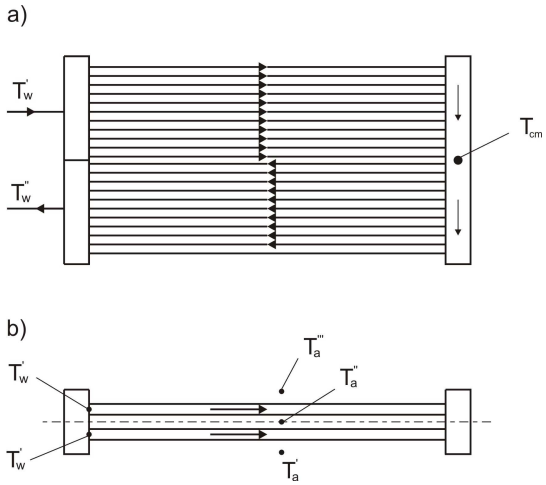

Figure 2: Diagram of two-row cross-flow heat exchanger (automotive radiator) with two passes; front view (a) and horizontal section of the upper pass (b), T_w – water temperature, T_a – air temperature

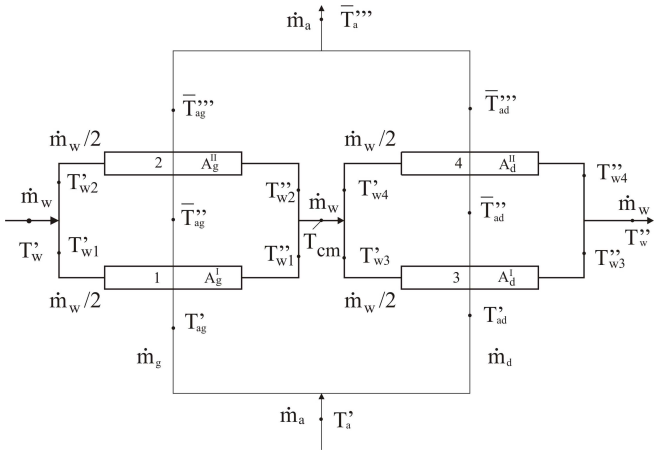

Figure 3: Flow diagram of two row cross-flow heat exchanger (automotive radiator) with two passes; 1 – first tube row in upper pass, 2 – second tube row in upper pass, 3 – first tube row in lower pass, 4 – second tube row in lower pass

4. Prediction of correlations for the air-side Colburn *j*-factor

A new experimental-numerical technique, based on two different methods for determining air-side heat transfer coefficient h_a , is developed for the estimation of the thermal contact resistance between the tube and fins. Two methods for determining the correlations for Colburn *j*-factor are presented. The first experimental-numerical method requires the experimental data. The second is based on the CFD simulation of flow and heat transfer in the heat exchanger.

4.1. Experimental-numerical method

The heat transfer coefficient h_{in} on the water-side is known, while the heat transfer coefficient on the air-side h_a is to be found. The following parameters are known from the measurements: liquid volumetric flow rate $\dot{V}_w$, air velocity w_0, inlet liquid temperature f'_w, inlet air temperature f'_a, outlet liquid temperature f''_w. The construction of the heat exchanger and the materials of which it is made are also known. The average heat transfer coefficient h_{in} on the inner surface of the tube was calculated using the Gnielinski correlation [10] for turbulent flow

$$Nu_w = \frac{\xi/8\,(\,\mathrm{Re}_w - 1000\,)\,\mathrm{Pr}_w}{1+12.7\,(\,\xi/8\,)^{1/2}\,(\,\mathrm{Pr}_w^{2/3}-1\,)}\left[\,1+\left(\,\frac{d_t}{L_t}\,\right)^{2/3}\,\right] \tag{5}$$

where $Nu_w = h_{\text{in}}\, d_t/k_w$, $Re_w = w_w\, d_t/\nu_c$ and $Pr_w = \mu_w\, c_{pw}/k_w$ are the water-side Nusselt, Reynolds and Prandtl numbers, respectively, and ξ is the friction factor given by

$$\xi = \frac{1}{(\,1.82\log \mathrm{Re}_w - 1.64\,)^2} = \frac{1}{(\,0.79\ln \mathrm{Re}_w - 1.64\,)^2} \tag{6}$$

The value of the air-side heat transfer coefficient $h^e_{a,i}$ is determined from the condition that the calculated water outlet temperature $T''_{w,i}(h^e_{a,i})$ must be equal to the measured temperature $f''_{w,i}$, where $i=1,...,n$ denotes the data set number. The following non-linear algebraic equation has to be solved for each data set to determine $h^e_{a,i}$

$$f''_{w,i} - T''_{w,i}\left(\,h^e_{a,i}\,\right) = 0, \quad i = 1,...,n \tag{7}$$

where n denotes the number of data sets. In order to calculate the water outlet temperature $T''_{w,i}$ as a function of the heat transfer coefficient $h^e_{a,i}$, the analytical mathematical model of the heat exchanger developed in [11] was used. The heat transfer coefficient on the air-side $h^e_{a,i}$ was determined by searching the preset interval so that the measured outlet temperature of the water $f''_{w,i}$ and the computed outlet temperature $T''_{w,i}$ are equal. The outlet water temperature $T''_{w,i}(h^e_{a,i})$ is calculated at every searching step. Next, a specific form was adopted for the correlation formula for the Colburn factor $j_a = j_a(Re_a)$ on the air-side, containing m unknown coefficients. The coefficients $x_1, x_2, ..., x_m$, $m \le n$ are determined using the least squares method from the condition

$$S = \sum_{i=1}^{n} \left[j^{e}_{a,i} - j_{a,i}\left(x_1, x_2, ..., x_m \right) \right]^2 = \min \quad m \le n \tag{8}$$

where

$$j_a = Nu_a / (\mathrm{Re}_a \, \mathrm{Pr}_a^{1/3}) \tag{9}$$

denotes the Colburn factor and $Pr_a = \mu_a \, c_{pa} / k_a$ is the Prandtl number. The dimensionless quantities $Nu_a = h_a \, d_h / k_a$ and $Re_a = w_{max} \, d_h / \nu_a$ stand for the air-side Nusselt and Reynolds numbers, respectively. The velocity w_{max} is the air velocity in the narrowest free flow cross-section A_{min}. The symbol $j^{e}_{a,i}$ denotes the experimentally determined value of the factor, and $j_{a,i}$ the calculated factor value which results from the adopted approximating function for the set value of the Reynolds number $Re_{a,i}$. The Colburn factor j_a was approximated by the power-law function

$$j_a = x_1 \, \mathrm{Re}_a^{x_2} \tag{10}$$

The unknown coefficients x_1 and x_2 are determined by the Levenberg-Marquardt method (Seber and Wild, 1989) using the Table-Curve program [13]. Combining Equations (9) and (10), one obtains

$$Nu_a = x_1 \, \mathrm{Re}_a^{(1+x_2)} \, \mathrm{Pr}_a^{1/3} \tag{11}$$

All the air properties that appear in the dimensionless numbers are evaluated at the average temperature taken from the inlet temperature T'_{am} and outlet air temperature T''_{am}.

4.2. Determination of the Colburn *j*-factor on the air-side based on the CFD simulation

In order to determine the heat transfer coefficients and then Colburn *j*-factors, the air temperature differences must be calculated first using the CFD simulation of flow and heat transfer on the air side.

4.2.1 Numerical simulation

In order to determine the 3D flow and heat transfer in the air and heat conduction through the fins and tubes, the problem will be studied numerically. In this paper, the air and heat flow in the tested two-row automotive radiator was simulated numerically by using the CFD program FLUENT [14].

The three-dimensional (3D) flow is treated as turbulent, since the air-side Reynolds number Re_a, before the heat exchanger is greater than 10000. Owing to the complicated construction of the radiator, the numerical study of the whole radiator is very difficult to perform (Fig. 3). Therefore, due to the symmetry, the 3D flow through the single narrow passage between the fins was simulated. The temperature distribution in the adjacent plate fins and tube walls was also calculated. In this way, the effect of non-uniform heat transfer coefficient on the tube and fin surfaces is taken into account, as well as the effect of the tube-to-tube heat conduction through the fins on the heat transferred from the water to the air. Fig. 4 shows the measurement data set No.7 from Table 1 taken as the input data. The thermal contact resistance between the tube and fins was modelled by inserting a thin layer of material with known thickness of 0.01 mm (Fig. 5).Thermal conductivity of the layer was varied to adjust the function $j(\mathrm{Re_a})$ obtained from the CFD simulation to the function $j(\mathrm{Re_a})$ based on experiments.

The computations were conducted for the 10 data sets. The uniform frontal velocity w_0 and uniform temperature T'_a in front of the radiator were assumed. The boundary condition of the third kind (convection surface condition) is specified at the inside surface S_{in} of the oval tubes (Fig. 4)

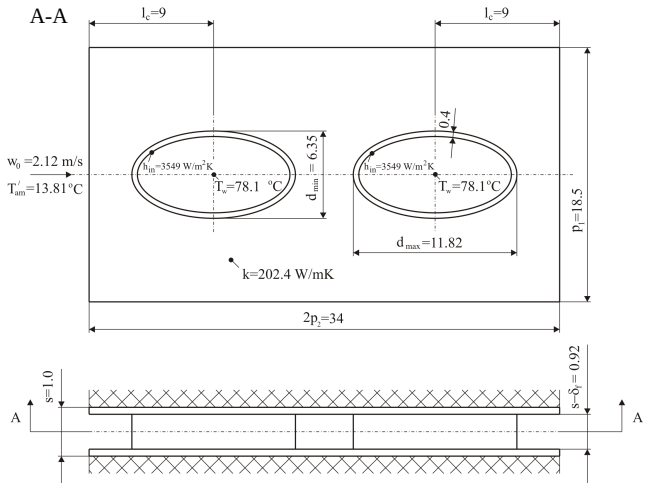

Figure 4: Single narrow passage between the fins simulated using CFD code – repeatable segment of the two-row plate fin and tube heat exchanger configuration; the dimensions are given in millimeters

$$-k_t \left(\partial T_t / \partial n\right)\big|_{S_{in}} = h_{in}\left(T_t\big|_{S_{in}} - T_w\right) \tag{12}$$

The symbol *n* denotes normal direction to the inside tube surface. The water-side heat transfer coefficient h_{in} was calculated from Equation (5). The inlet temperature of the water T_w was taken as the bulk water temperatures at the first and second row of tubes. where k_t is the tube's thermal conductivity, T_t and T_w are the temperatures of the tube and water, respectively.

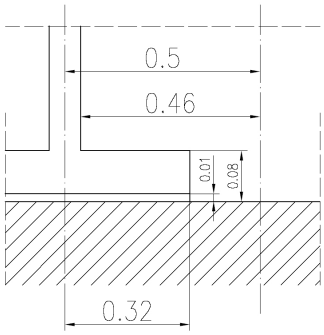

Figure 5: Longitudinal section of the fin-to-tube attachment - thin layer with thickness of 0.01 mm and known thermal conductivity simulates the thermal contact resistance between the tube and fin

The flow passage between the fins is divided into twenty layers of finite volumes, while only two layers constitute half of the thickness of the fin. Only the quarter of the passage shown in Fig.4 was simulated. The mesh of finite volumes with 578 864 nodes is shown in Fig.6.

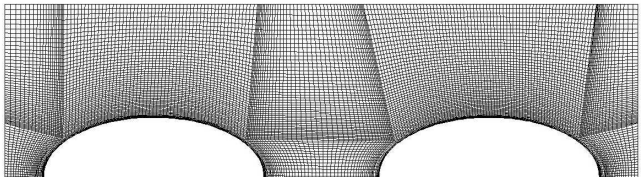

Figure 6: Mesh of finite control volumes

The simulation reveals high values of the heat flux on the fin's leading edge due to the developing air flow. Near the fin surface, the temperature of the air increases in the flow direction and causes a corresponding reduction in the heat flux. Stagnation flow on the front of the tube in the first row produces high heat transfer near the base of the fin and at the frontal part of the tube circumference. Behind the tubes, low-velocity wake regions exist. In the downstream regions of the tubes, low air velocities and very low heat fluxes can be observed in the first and second row. Relatively low heat fluxes are encountered on the portions of the fin that lie downstream of the minimum flow cross sections. The heat transfer rates are especially low in the recirculation regions behind the tubes. In the regions with small air velocities, the air temperatures are large. The larger part of the total heat transfer rate is transferred in the first tube row. The key to heat transfer enhancement on the fin associated with the first tube row is a major contribution of the developing flow region, while the portion of the fin adjacent to the second tube row has no developing flow contribution and only a weak vortex contribution.

4.2.2 Determination of the Colburn j-factor

The second method is based on the CFD simulation of fluid flow and heat transfer in the heat exchanger. Although the temperature and heat flux distributions on the tube and fin surfaces are known from this simulation, the local and average heat transfer coefficients are difficult to determine because it is unclear what air temperature should be assumed as the bulk air temperature. The presented method circumvents this problem and allows for determining the mean air-side heat transfer coefficient. The heat transfer coefficient h_a is determined from the condition that temperature increase of the air ΔT_t over two rows of tubes (over the heat exchanger) calculated using the analytical model of the heat exchanger is equal to the temperature increase obtained from the numerical simulation using FLUENT. Since the temperature distribution at the inlet and outlet of the modelled passage is two-dimensional, then the mass average air temperature difference $\Delta\overline{T}_t$ computed by Fluent should be equal to the air temperature difference ΔT_t calculated using an analytical model of the heat exchanger

$$\Delta T_{t,i}\left(h_{a,i}\right) - \Delta\overline{T}_{t,i} = 0\ ,\quad i = 1,...,n \tag{13}$$

The temperature difference ΔT_t is given by the expression:

$$\Delta T_t = T_a''' - T_a' = \Delta T_I + \Delta T_{II} \tag{14}$$

where $\Delta T_I = T_a'' - T_a'$ and $\Delta T_{II} = T_a''' - T_a'$ represent the air temperature increase over the first and second tube row, respectively (Fig. 7).

The mean value of the heat transfer coefficient $h_{a,i}$ over two tube rows is determined by solving Equation (13). Determining the heat transfer coefficients can be significantly simplified if we take into account that the water temperature has no large influence on the searched heat transfer coefficients because air properties are not influenced substantially by temperature. Thus, the equal water temperature T_w (Fig. 7) at the first and second row of tubes may be assumed. If the temperature of the water flowing inside the two tube rows is constant, then the air temperature T_a in the first and second tube rows can be obtained from the solution of the differential equations:

$$\frac{d\,T_a\left(y_I^+\right)}{d\,y_I^+} = N_a^I\left[\,T_w - T_a\left(y_I^+\right)\right] \tag{15}$$

$$T_a\Big|_{y_I^+=0} = T_a' \tag{16}$$

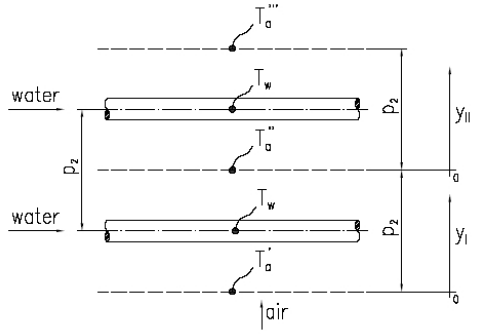

Figure 7: Cross-flow heat exchanger with two rows of tubes

$$\frac{d\,T_a\left(y_{II}^+\right)}{d\,y_{II}^+} = N_a^{II}\left[\,T_w - T_a\left(y_{II}^+\right)\right] \tag{17}$$

$$T_a\Big|_{y_{II}^+=0} = T_a'' \tag{18}$$

Solution of the initial-boundary problems (15-16) and (17-18) simplifies to:

$$T_a\left(y_I^+\right) = T_w + \left(T_a' - T_w\right)e^{-N_a^I\,y_I^+} \tag{19}$$

$$T_a\left(y_{II}^+\right) = T_w + \left(T_a' - T_w\right)e^{-\left(N_a^I + N_a^{II}\,y_{II}^+\right)} \tag{20}$$

where

$N^I{}_a = U^I{}_a\,A/(\dot m_a\,c_{pa})$, $N^{II}{}_a = UI^I{}_a\,A/(\dot m_a\,c_{pa})$.

The air temperatures $T_a(y_I^+)$ and $T_a(y_{II}^+)$ at the first and second tube rows, respectively, do not depend on the x coordinate, since the fluid temperature T_w in both tube rows is constant. The differences of the air temperature over the first and second tube rows are given by:

$$\Delta T_I = T_a\Big|_{y_I^+=1} - T_a\Big|_{y_I^+=0} = \left(T_w - T_a'\right)\left(1 - e^{-N_a^I}\right) \tag{21}$$

$$\Delta T_{II} = T_a\Big|_{y_{II}^+=1} - T_a\Big|_{y_{II}^+=0} = \left(T_w - T_a'\right)e^{-N_a^I}\left(1 - e^{-N_a^{II}}\right) \tag{22}$$

If the air-side heat transfer coefficients at the first and second rows are assumed to be equal, i.g. $N_a = N_a{}^I = N_a{}^{II}$, then the total temperature difference ΔT_i over two rows simplifies to

$$\Delta T_t = \Delta T_I + \Delta T_{II} = \left(T_w - T_a'\right)\left(1 - e^{-2\,N_a}\right) \tag{23}$$

The air temperature increase ΔT_t is the function of the unknown heat transfer coefficient h_a .

5. Test facility

The measurements were carried out in an open aerodynamic tunnel. The experimental setup was designed to obtain heat transfer and pressure drop data from commercially available automotive radiators. The test facility (Fig. 8) follows the general guidelines presented in ASHRAE Standards 33-798 and 84-1991. Air is forced through the

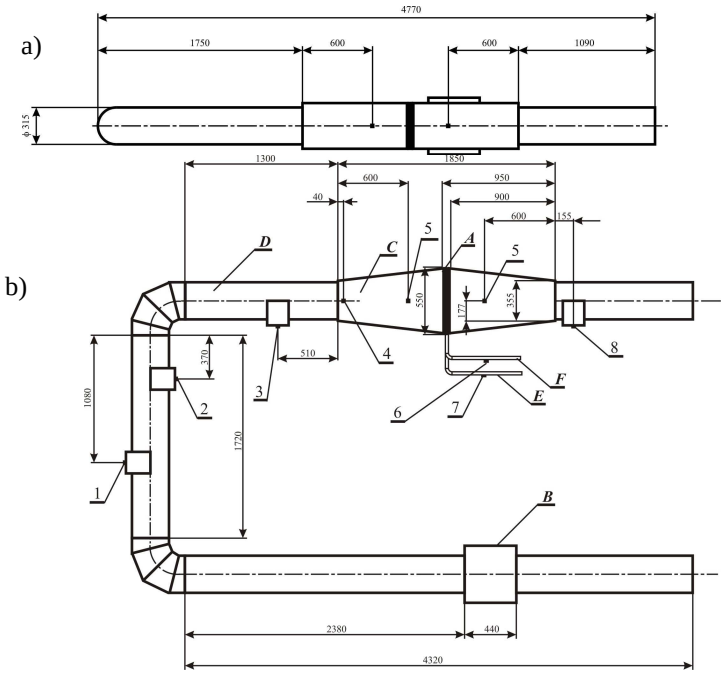

Figure 8: Open-loop wind tunnel for experimental investigations of the tube-and-fin heat exchanger (car radiator); (a) front view, (b) top view; A – car radiator, B – variable speed centrifugal fan, C – chamber with car radiator, D – pipe with outer diameter of 315 mm and wall thickness of 1 mm, E – water outlet pipe, F – water inlet pipe,1 – measurement of the mean and maximum air velocity using a Pitot-static pressure probe, 2 – measurement of the mean and maximum air velocity using a turbine velocity meter with head diameter of 11 mm, 3 – measurement of the mean and maximum air velocity using turbine velocity meter with head diameter of 80 mm, 4 – air temperature measurement before the car radiator, 5 – measurement of pressure drop over the car radiator, 6 – water temperature at radiator inlet, 7 – measurement of water temperature at radiator outlet, 8 – air temperature measurement after the car radiator

open-loop wind tunnel by a variable speed centrifugal fan. The air flow passed the whole front cross-section of the radiator. A computer-based data-acquisition system was used to measure, store and interpret the data. The relative difference between the air-side and liquid-side heat transfer rate was less than 3%. Heat transfer measurements under steady-state conditions were conducted to find the correlation for the air-side Colburn *j*-factor number.

6. Results

The temperature difference over the radiator obtained from the CFD simulation without the thermal contact resistance between the tube and fins is larger than that obtained from the analytical heat exchanger model, in which the experimental correlations for heat transfer coefficients are used. The lower values of the air temperature difference across the radiator obtained from the analytical model of the heat exchanger, may result from the contact resistance between the fins and the tubes. In order to show the influence of the thermal contact resistance on the temperature differences, ΔT_I, ΔT_{II} and ΔT_t, CFD simulations using FLUENT were conducted for various values of the gap effective thermal conductivity k_g (Fig. 9).

The velocity and temperature of the air before the radiator was 2.12 m/s and 286.96 K, respectively. The water temperature in both tube rows was 351.25 K. The CFD simulation was performed using the commercial CFD software FLUENT for h_{in} = 3549 W/(m^{2}K). An inspection of the results shown in Fig. 9 indicates that for the thermal conductivity k_g > 1 W/(mK) (g / k_g = 0.00001/1 = 0.00001 m^{2}K/W) the temperature differences are almost independent on the gap thermal resistance g / k_g . In addition, it has been found from the numerical CFD simulation that the fins and tubes in the second row are less effective than those in the first row. The temperature difference over the first tube row is almost three times larger than the second tube row (Fig. 9). The key to heat transfer enhancement on the fin associated with the first tube row is a major contribution of the developing boundary layer on the inlet part of the fins, while the portion of the fin adjacent to the second tube row has no boundary layer contribution and only a small vortex contribution. The heat transfer at the forward stagnation points on the first tube row is also intensive. The regions behind the tubes contribute very little to the performance of the heat exchanger. The thermal measurements results for the automotive radiator are shown in Table 1.

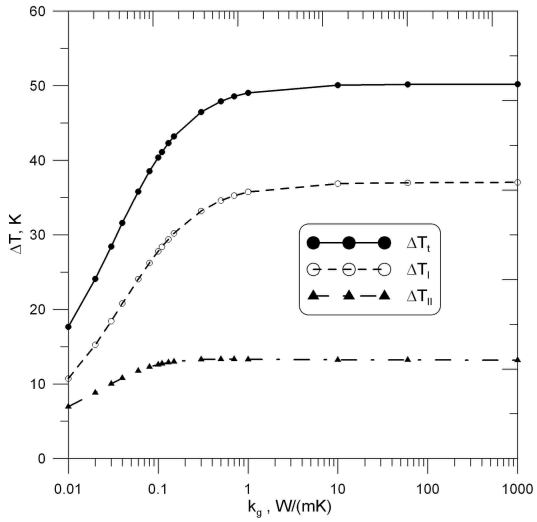

Figure 9: Effect of effective thermal conductivity of the gap between the tube and fins on air temperature differences over the first ΔT_I, second ΔT_{II} , and over the entire car radiator ΔT_t

Correlations for the air-side Colburn *j*-factors for an automotive radiator were determined using the method described above. The comparisons of correlations $j_a(Re_a)$ for the entire heat exchanger are shown in Fig. 10. The black dots in Fig. 10 represent values of $j_{a,i}(Re_{a,i})$, in which the air-side heat transfer coefficient was determined based on the measured temperatures of water at the outlet of the heat exchanger (Table 1). The water-side heat transfer coefficients h_{in} were calculated using the Gnielinski correlation (5).

Table 1. Measurement data for the automotive radiator

No.	w_0 [m/s]	$\dot{V}_w$ [L/h]	$T_a^{'}$ [°C]	$T_w^{'}$ [°C]	$T_w^{''}$ [°C]	Re_a	Re_w
1	0.96	551.5	0.73	85.44	65.11	155	2956
2	1.21	735.2	10.54	83.97	67.78	187	3970
3	1.45	736.4	10.49	87.64	68.67	223	4088
4	1.61	736.9	10.47	82.63	63.98	250	3855
5	1.77	1257	12.41	79.72	67.35	271	6592
6	1.76	736.3	10.41	83.36	63.57	273	3859
7	2.12	1272	13.81	78.15	65.17	323	6516
8	2.12	1269	12.63	78.92	65.49	325	6545
9	2.11	734.9	11.04	85.10	63.00	328	3880
10	2.13	734.1	11.04	83.09	61.64	331	3795

The solid line in Fig. 10 represents the least squares approximation based on the 10 data series:

$$j_a = 0.1386\,\mathrm{Re}_a^{-0.3897} \tag{24}$$

from which the correlation for the air-side Nusselt number results

$$Nu_a = 0.1386\,\mathrm{Re}_a^{0.6103}\,\mathrm{Pr}_a^{1/3} \tag{25}$$

In the correlation (25) contact resistance between the tube and fin is implicitly included in the air-side heat transfer coefficient, which was determined using the first method. The other plots in Fig. 10 are based on the CFD simulation using FLUENT. The same 10 data series, as in the method I, were used in the CFD simulation. The correlations were obtained under the assumption that the air flow was laminar. Only the air-side heat transfer coefficient h_a is determined from the condition that the air temperature increase across the heat exchanger obtained from the CFD simulation is equal to the temperature increase calculated using Equation (23). The water-side heat transfer coefficient h_{in} is calculated using the Gnielinski correlation (5). The results presented in Fig. 10 show significant influence of the thermal contact resistance on the determined $j_a(Re_a)$ curve. The lower is the effective thermal conductivity k_g of the gap the smaller is the Colburn factor j_a. The best agreement between the experimental curve $j_a(Re_a)$ and the curve based on the CFD simulation was obtained for k_a = 0.12 W/(mK) (Fig. 10). Thus, it can be concluded that the effective thermal conductivity of the gap is about 0.12 W/(mK) and thermal contact resistance $g/k_g = 0.00001/0.12 = 8.33 \cdot 10^{-5}\ m^2K/W$.

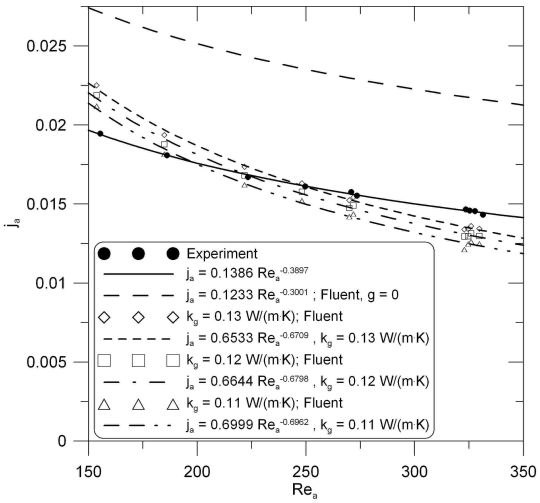

Figure 10: Colburn j_a - factor for the investigated car radiator

Having determined the heat transfer coefficients $h_{a,i}$ i = 1,…,n, from the solution of the non-linear algebraic equation (13), the heat transfer correlations are derived in the same way as in the method I. First, the $j_{a,i}$ are calculated for i = 1,…,n using equation (9), and then the obtained results are approximated by the function (10), using the least-squares method.

7. Conclusions

Two different methods were used to determine correlations for the air-side Colburn *j*-factors. The first method is based on the experimental data while the second is based on the CFD simulation of the flow and heat transfer in the heat exchanger. In the first method, the air-side heat transfer coefficient was determined from the condition that the calculated and measured liquid outlet temperatures are equal. The heat transfer coefficient on the tube-side was calculated using the Gnielinski correlation. An analytical model of the heat exchanger was used to calculate the water and air outlet temperatures as the function of the searched heat transfer coefficients.

The second method for determining air-side heat transfer correlations, based on the CFD simulation of flow and heat transfer and on the simplified analytical model of heat transfer in the heat exchanger, was proposed. Based on the calculated heat transfer coefficients, the dimensionless correlation for the Colburn *j*-factor as a function of the Reynolds number can be found. The thermal contact resistance between the tube and fins was estimated by comparing the experimental and CFD based $j_a(Re_a)$ plots. The CFD programs can also be used for calculating mean heat transfer coefficients over a specified tube row.

Nomenclature

A	area, m^2
c_p	specific heat at constant pressure, J/kgK
d	diameter, m
d_{in} , d_o	inner and outer tube diameter, m
f	measured temperature, °C or K
F	correction factor, dimensionless
g	thickness of the gap between the tube and fin, m
h	heat transfer coefficient, W/m^2K
$\bar{h}$	enhanced heat transfer coefficient based on the tube outer surface A_o, W/m^2K
j	Colburn j-factor, $Nu/Re\ Pr^{1/3}$, dimensionless
k	thermal conductivity, W/mK
L_t	tube length in the car radiator, m
m	number of unknown coefficients, dimensionless
$\dot{m}$	mass flow rate, kg/s
n	data set number, dimensionless
N	number of transfer units, $N = U_o A/(\dot{m}\ c_p)$, dimensionless
Nu	Nusselt number, dimensionless
p_f	fin pitch, m

p_1 pitch of tubes in plane perpendicular to flow, m
p_2 pitch of tubes in direction of flow, m
P perimeter, m
Pr Prandtl number, dimensionless
R contact thermal resistance between tube and fin, m^2K/W
Re Reynolds number, dimensionless
T temperature, °C or K
U overall heat transfer coefficient, W/m^2K
$\dot{V}$ volume flow rate, m^3/s
w velocity, m/s
x, y Cartesian coordinates, m
x_i unknown coefficient, dimensionless
y_I^+, y_{II}^+ dimensionless coordinate, $y_I^+ = y_I/p_2$, $y_{II}^+ = y_{II}/p_2$
δ thickness, m
ΔT temperature difference, K
η fin efficiency, dimensionless
μ dynamic viscosity, Ns/m^2
ν kinematic viscosity, m^2/s
ξ Darcy-Weisbach friction factor, dimensionless

Subscript

a air
f fin
g gap
in inner
m logarithmic mean temperature difference
o outer
t tube
w wall
I, II first and second tube row, respectively

Superscript

e experimental
’ inlet
’’ outlet

References

[1] D. M. Dart, *Effect on Fin Bond*, ASHRAE Trans, Vol. 1, pp. 67-71, 1959.
[2] J. W. Sheffield, R. A. Wood, H. J. Sauer, *Experimental Investigation of Thermal Conductance of Finned Tube Contacts*, Experimental Thermal and Fluid Science, Vol. 2, pp. 107-121, 1989.
[3] J. Jeong, Ch. N. Kim, B. Youn, Y. S. Kim, *A Study of the Correlation between the Thermal Contact Conductance and Effective Factors in Fin-Tube Heat Exchangers with 9.52 mm Tube*, Int. J. Heat and Fluid Flow, Vol. 25, pp. 1006-1014, 2004.
[4] J. Jeong, Ch. N. Kim, B. Youn, *A Study on the Thermal Contact Conductance in Fin-Tube Heat Exchangers with 7mm Tube*, Int. J. Heat and Mass Transfer, Vol. 49, pp. 1547-1555, 2006.
[5] A. D. Kraus, A. Aziz, J. Welty, *Extended Surface Heat Transfer*, John Wiley & Sons, New York,2001.
[6] J. Taler, P. Duda, *Solving Direct and Inverse Heat conduction Problems*, Springer, Berlin, 2006.
[7] G. F. Hewitt, G. L. Shires, T. R. Bott, *Process Heat Transfer*, CRC Press, Boca Raton, 1994.
[8] F. C. McQuiston, J. D. Parker, J. D. Spitler, *Heating, Ventilating, and Air Conditioning*, Sixth Edition, John Wiley and Sons, New York, 2005.
[9] W. M. Kays and A. L. London, *Compact Heat Exchangers*, 3rd ed., McGraw-Hill, New York, 1984.
[10] V. Gnielinski, *Neue Gleichungen für den Wärme- und den Stoffübergang in turbulent durchströmten Rohren und Kanälen*, Forschung im Ingenieurwesen, Bd. 41, Nr. 1, pp. 8-16, 1975.
[11] D. Taler, *Determination of heat transfer correlations for plate-fin-and-tube heat exchangers*, Heat and Mass Transfer, Vol. 40, pp. 809-822, 2004.
[12] G. A. F. Seber, C. J Wild, *Nonlinear Regression*, John Wiley & Sons, New York, 1989.
[13] Table Curve, *Automated Curve Fitting Software*, AISN Software, Chicago, 2005
[14] FLUENT 6.0., *Fluent Inc.*, 10 Cavendish Court, Lebanon, NH03766, USA, 2003
[15] D. Taler, *Measurements of Pressure, Velocity and Mass Flow Rate of Fluids*, University of Science and Technology Press (UWND AGH), Cracow (in Polish), 2006